# Experimental and Numerical Study of the Emitter Turn-Off Thyristor (ETO)

Yuxin Li, *Student Member, IEEE*, Alex Q. Huang, *Senior Member, IEEE*, and Kevin Motto

***Abstract*—The emitter turn-off thyristor (ETO) is a new family of high power semiconductor devices that is suitable for megawatt power electronics application. ETO's with voltage and current ratings of 4–6 kV and 1–4 kA, have been developed and demonstrated. And those power levels are the highest in silicon power devices and are comparable to those of the gate turn-off thyristor (GTO). Compared to the conventional GTO, the ETO has much shorter storage time, voltage controlled turn-off capability, and much larger reverse biased safe operation area (RBSOA). Furthermore, ETO's have a forward-biased safe operation area (FBSOA) that enables it to control the turn-on $di/dt$ similar to an insulated gate bipolar transistor (IGBT). These combined advantages make the ETO based power system simpler in terms of $dv/dt$ snubber, $di/dt$ snubber, over current protection, resulting in significant savings in the system cost. This paper presents experimental and numerical results that demonstrate the advantages of the ETO.**

***Index Terms*—Gate turn-off thyristor, hard-driven, snubberless turn-off.**

## I. Introduction

THYRISTOR technology has long been the only solution to megawatt power applications. The combined index of its forward voltage drop, blocking voltage and conducting current is the best among power semiconductor devices. By adding gate turn-off capability, the gate turn-off thyristor (GTO) has found applications in HVDC, traction and megawatt drive systems. However, the GTO has several drawbacks. The inhomogeneous current distribution during the turn-on transient results in the $di/dt$ problem and demands a turn-on $di/dt$ limiting snubber. The P-N-P-N four-layer structure makes the GTO sensitive to $dv/dt$ induced turn-on, so a $dv/dt$ limiting snubber is also needed for device turn-off. The inhomogeneous transient current distribution is also the major reason for a small reverse-bias-safe-operation-area (RBSOA) in GTO's. A large derating factor has to be used in practical applications. Another major problem of the GTO is that a complicated gate driver consuming hundreds of watts is needed in a typical application. These gate drivers are usually bulky and have very slow transient response, resulting in a very long storage time. The operation frequency of the GTO is therefore limited to less than 500 Hz.

Recent developments of high power IGBT's [1] are challenging the dominant position of GTO's in megawatt applications due to their high speed, large RBSOA and ease of control. However, the available voltage/current rating of IGBT's is still lower than that of GTO's. This situation may continue in the foreseeable future. To meet the demand for advanced high power semiconductor devices, many efforts have been made to improve the GTO-oriented device in the past few years. Among these efforts are the MOS turn-off (MTO) [2] thyristor and the integrated gate commutated thyristor (IGCT) [3]. With dramatically improved speed and dynamic performance, these GTO-based devices will help maintain the dominance of GTO technology in high power areas.

The emitter turn-off thyristor (ETO) [4], [5] is another major effort in the development of GTO-technology-based high power semiconductor devices. Based on mature technologies of the GTO and power MOSFET, the ETO provides a low cost and superior solution to megawatt applications. Theoretical analysis and experimental results suggest that the ETO have the combined advantages of both the GTO and the MOSFET.

1) GTOs' high voltage/current ratings, low forward voltage drop.
2) Voltage turn-off capability similar to an IGBT.
3) High switching speed.
4) Wider RBSOA.
5) Existence of FBSOA.

High power ETO's with current ratings of 1–4 kA, and voltage ratings of 1–6 kV have already been demonstrated at the Center for Power Electronics System, Virginia Tech. In this paper, the operation principles of the ETO, its switching performance, unity turn-off gain characteristic, snubberless turn-off capability, and its comparison with the IGBT and IGCT are presented.

## II. Operation Principles of the ETO

Three main characteristics of the traditional GTO have to be improved in order to accommodate the need of high frequency high power conversion applications. First, the bulky, power consuming gate driver has to be eliminated. This can be achieved if a voltage-controlled device is introduced. Second, the RBSOA of the GTO has to be improved to make a robust device. The RBSOA of traditional GTO's is limited by the current filamentation and crowding problems because each of the GTO's cells has a different storage time [6], which generates nonuniform current distribution during device turn-off. Significant derating is therefore required, resulting in a small RBSOSA. Third, the overall speed of the GTO has to be improved. This requires the reduction of the storage time, current fall time and tail time, and improvement in $dv/dt$ and $di/dt$ capability. These transient

Manuscript received April 13, 1999; revised October 1, 1999. This work was supported by Sandia National Lab, Westcode Semiconductor Inc., the Office of Naval Research, and the National Science Foundation under Award EEC-9731677. Recommended by Associate Editor, W. M. Portnoy.

The authors are with the center for Power Electronics Systems, Virginia Polytechnic Institute and State University, Blacksburg, VA 24061 USA.

Publisher Item Identifier S 0885-8993(00)03385-8.

0885-8993/00$10.00 © 2000 IEEE

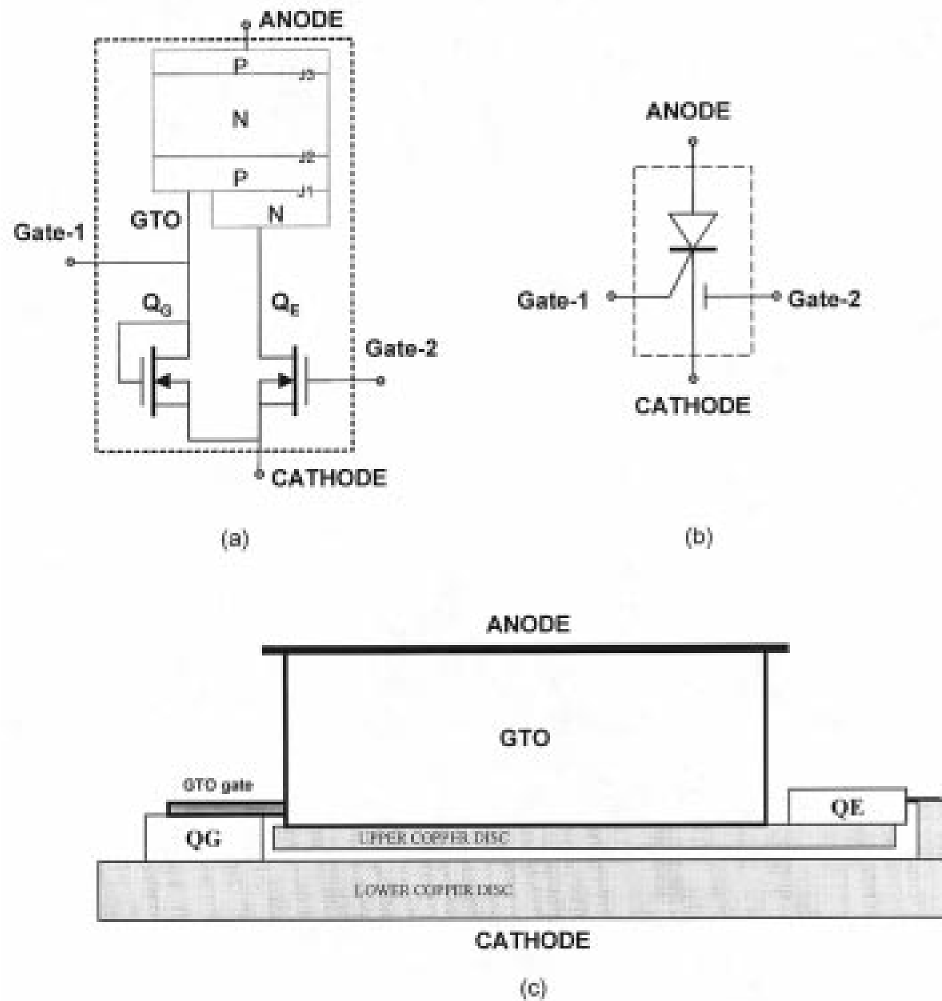


Fig. 1. (a) The ETO equivalent circuit, (b) the ETO symbol, and (c) the cross section of the ETO mechanical structure.

process times also determine the minimum ON/OFF time requirement of the GTO.

### A. Operation Principles

The emitter turn-off thyristor (ETO) is a MOS-GTO hybrid [4], [5], [7]–[9] device that is targeted to solve all these problems. Fig. 1 shows the equivalent circuit of the ETO. An emitter switch $Q_E$ is in series with the GTO, and a gate switch $Q_G$ is connected to the GTO's gate.

By turning on $Q_E$ and off $Q_G$, an injection current into the GTO gate(gate-1) can turn on the ETO. The traditional turn-on current is still necessary for the ETO due to the existence of the GTO. By turning off $Q_E$ and on $Q_G$, the GTO cathode current path is cut off and the cathode current has to commutate to the gate switch $Q_G$ via the GTO's gate, which finally turns off the ETO. It is therefore obvious, by using a MOSFET as the emitter switch, that the turn-off process is a voltage-controlled one. The turn-off current required by the GTO is supplied by itself instead of by an external gate driver.

It is very important to mention that both the emitter switch $Q_E$ and the gate switch $Q_G$ are not subjected to high voltage stress, no matter how high the voltage is on the ETO. The internal structure of the GTO's gate-cathode is a PN junction. In the ETO off state, the high voltage is blocked by the GTO's main junction $J_2$, and the leakage current is bypassed by the gate switch $Q_G$, which is in the ON state. The voltage on the emitter switch $Q_E$ follows that on $Q_G$, is low. In the ETO on state, the emitter switch is ON, so the voltage on the gate switch $Q_G$ cannot exceed the voltage across the emitter switch plus the GTO gate-cathode PN junction forward voltage drop.

### B. Unity Turn-Off Gain and RBSOA

The turn-off gain for the GTO is defined as the anode current over the gate current when the GTO is turning off. Normally, the turn-off gain of the GTO is designed between 3 and 5, so that even one third to one fifth of the anode current can turn the GTO off. High turn-off gain saves the gating power requirement but imposes a detrimental effect on the GTO. While a small portion of the cathode remains in the PNPN latch-up mode, a high enough turn-off $dv/dt$ displacement current can act as additional gate injection current and maintain small GTO spots in conduction. Under this condition, the GTO current will rapidly become filamented, with only a small amount of cells conducting the total current. The combination of high current and high voltage in a small area causes the GTO to fail. Therefore a $dv/dt$ snubber is always needed in GTO applications. On

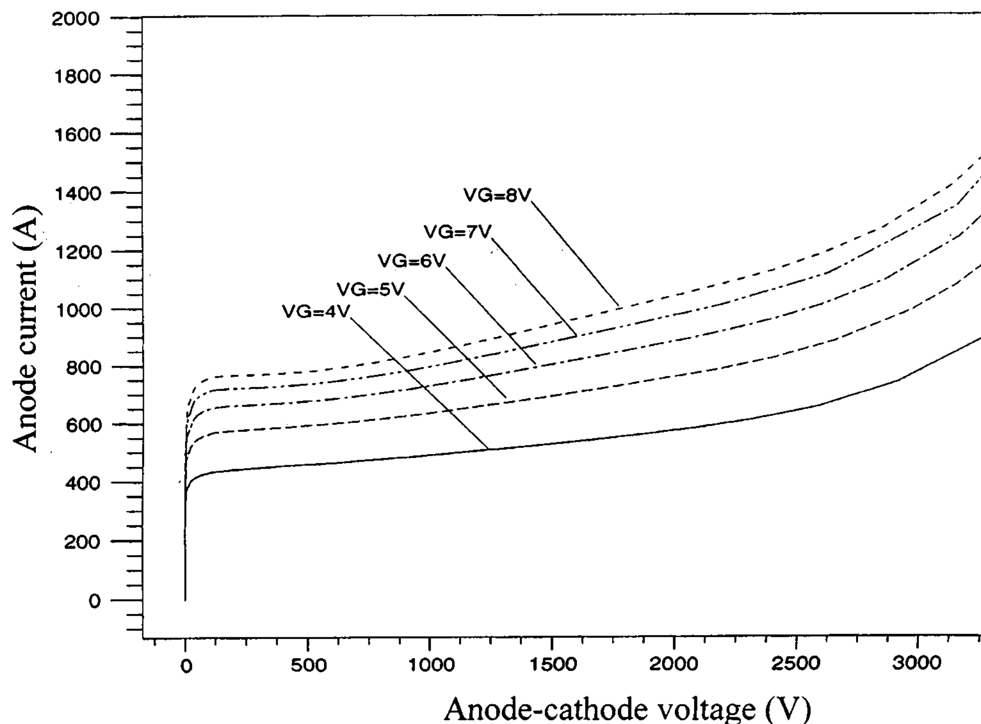


Fig. 2. High-voltage current saturation capability of the ETO obtained by device simulation.

the other hand, the turn-off gain in the ETO is unity. The time when the emitter switch $Q_E$ is turned off, the GTO cathode current has to commutate to its gate path. After the gate current commutation completes, the ETO is turned off with zero GTO cathode current, like an open base PNP transistor turn-off.

The unity turn-off gain benefits the ETO in several ways. First, the RBSOA of the GTO can be improved, so reduced $dv/dt$ snubber or even snubberless switching can be achieved. Under the unity turn-off gain condition [10], current filamentation cannot or is very hard to develop because lack of any positive feedback mechanism, and the RBSOA is only limited by the dynamic avalanche breakdown of junction $J_2$. The maximum RBSOA power-constant in the range of 200–300 kW/cm$^2$ has been reported for large area hard-driven GTO's [11]. Second, it can reduce the turn-off storage time significantly, since the much higher pull out current can quickly remove charges stored in the P-base of the GTO. The storage times of hard-driven or unity turn-off GTO's are typically in the range of 1–2$\mu$s [10].

### C. Mixed Mode Simulation and FBSOA

Besides the improvements expected in the RBSOA, speed and control, the ETO also has forward current saturation capability or Forward Biased Safe Operation Area (FBSOA). The FBSOA results from the ballasting effect of the emitter switch $Q_E$. Assuming the ETO gate switch $Q_G$ acts like a zener diode with an equivalent turn-on voltage of $V_Z$. Under normal conduction mode, the voltage on the emitter switch $Q_E$ is always less than ($V_Z$–$V_{J1}$), where $V_{J1}$ is the forward voltage drop across the GTO emitter junction, so the gate switch $Q_G$ is off, and the ETO's forward conduction behavior is similar to that of the GTO. However, by controlling the gate voltage, the emitter switch $Q_E$ can have a much higher voltage drop. Once this voltage is as high as ($V_Z$–$V_{J1}$), a portion of the GTO current will be diverted to the gate path. Because the current flowing out of the GTO gate has the effect of turning it off, the current conduction capability of the ETO decreases and the voltage drop across the ETO increases. This process continues until a balance is reached in which the anode current no longer increases with the increase of the ETO voltage.

Fig. 2 illustrates the high voltage/current saturation capability of the ETO obtained by two-dimensional mixed mode device simulation [12]. Fig. 3 shows the current flowlines of the ETO under the high voltage current saturation condition ($V_G = 7$ V, $V_{\text{anode}} = 2410$ V). It is clearly shown that part of the current flows out of the GTO's gate while another part of the current flows through the GTO's cathode. It is the current flowing out of the GTO's gate that results in the high-voltage current saturation characteristic of the ETO. Fig. 4 shows the potential contours of the ETO in the same case. The high voltage is supported by the main blocking junction—$J_2$, and the two transistors in the GTO are working in the linear active region instead of the saturation region.

The existence of the FBSOA in the ETO is a significant advantage over GTO's. FBSOA also exists in IGBT's and it benefits applications in two ways [13]. First, the dynamic $di/dt$ during the device turn-on can be controlled by the gate drive circuit. This will eventually eliminate the $di/dt$ snubber in high power system. Second, the FBSOA devices with the important self-current limiting and short circuit protection capabilities.

## III. Experimental Results of the ETO

Based on the operation principles and device simulation results, prototype ETO's, ranging from 1–4 kA, 4–6 kV, have been

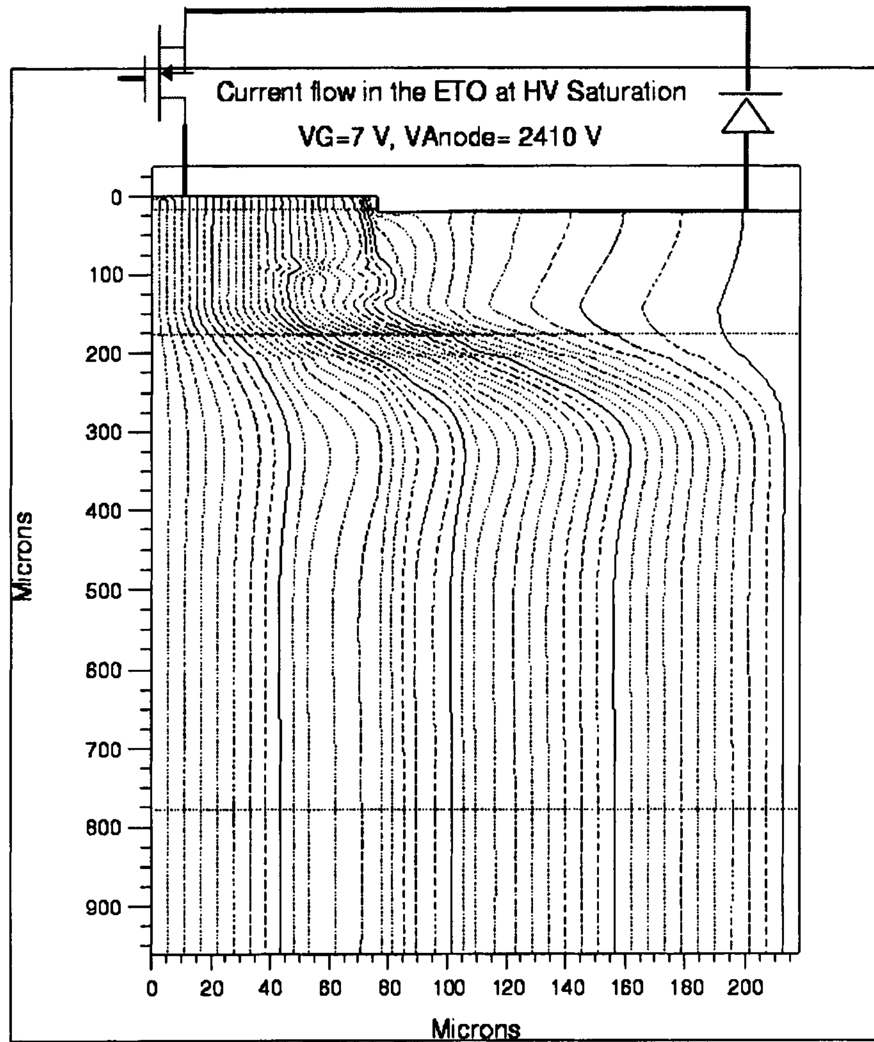


Fig. 3. Current flowlines of the ETO under high-voltage current saturation condition. Notice the current component toward the GTO gate.

developed. Fig. 5 shows the photograph of the developed ETO family along with their gate drivers. The model name of the ETO reflects the rating of the GTO used. The first two digits stand for the GTO's maximum turn-off current rating and the last two digits stand for the voltage rating. For example, ETO1045S means the GTO used for the ETO has a 1.0 kA turn-off current and a 4.5 kV voltage blocking capability.

Several practical issues have to be addressed in the development of these prototype models. First, it is difficult to realize an ideal emitter switch $Q_E$ and gate switch $Q_G$, as both of them are supposed to conduct the full anode current. Second, the stray inductance in the emitter-gate current commutating loop in practice determines whether the unity turn-off gain can be reached. That is to say, the stray inductance has to be reduced as much as possible. Many efforts have been made to optimize the design of the ETO with respect to the mechanical layout, electrical connection, thermal consideration, and current sharing.

The emitter switch $Q_E$ is realized by paralleling a number of high current low voltage n-channel power MOSFET's; the gate switch $Q_G$ is realized in the same way, by paralleling several MOSFET's. There are two ways to control the gate switch $Q_G$. One is to control it through a gate driver. This method provides the lowest gate impedance current path when $Q_G$ is on. The other way is to drive the gate switch by itself. By shorting its gate with the drain, the MOSFET acts as a two-terminal zener diode. The switch is off when the voltage on it is lower than the threshold voltage of the MOSFET, and is on when the voltage is higher. With the latter configuration, the ETO can withstand high $dv/dt$ even when its gate driver is not powered on because the gate switch $Q_G$ can be turned on automatically and passes $dv/dt$ displacement current. The positive temperature coefficiency of the majority carrier power MOSFET also ensures uniform current sharing among MOSFET's used for $Q_E$. The use of ultra low channel resistance of advanced MOSFET's minimizes the added forward voltage drop to the ETO.

Experimental results obtained from the developed ETO prototypes confirm the predicted high switching speed and short storage time. Fig. 6 shows a typical ETO turn-off characteristic obtained on a high power pulse tester. Table I summarizes the measured results of several 53 mm ETO's(ETO1045S) and

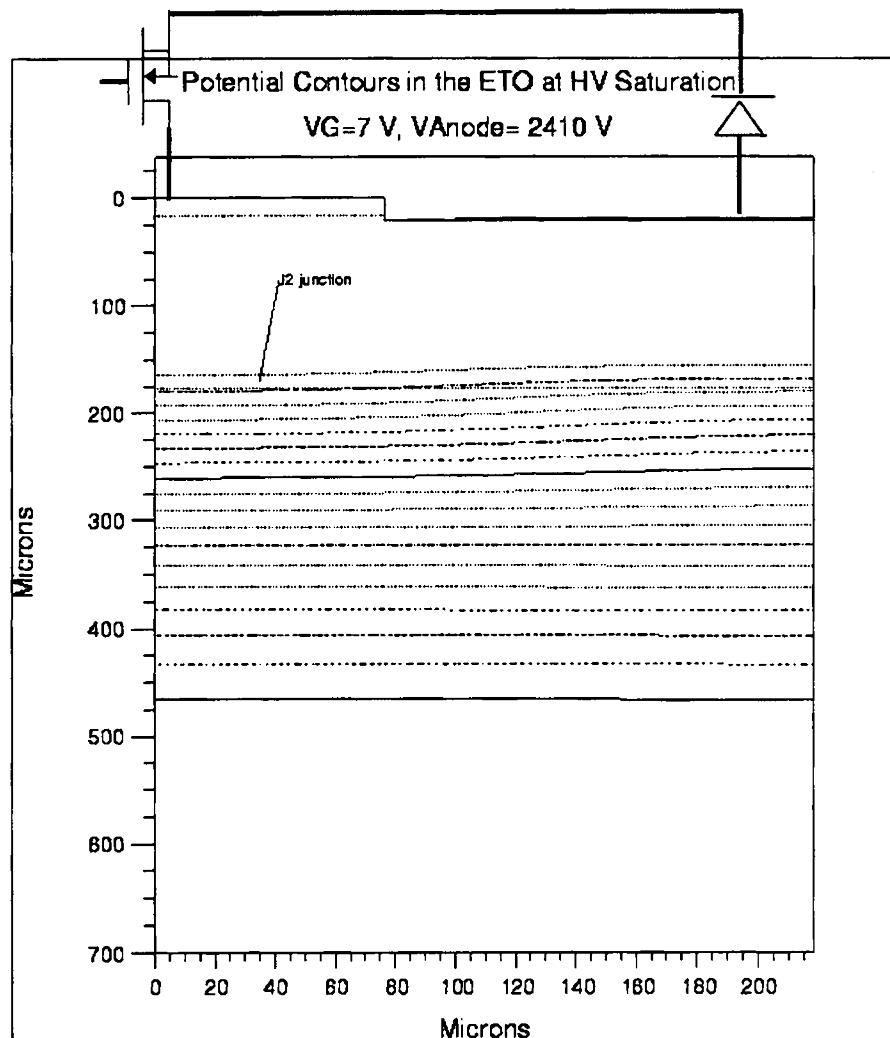


Fig. 4. Potential contours of the ETO under high-voltage current saturation condition. High voltage is supported by the blocking junction J2.

GTO's. Table II summaries the turn-off parameters of three different types of ETO's. Compared with the GTO, the storage times of the ETO are dramatically reduced from typically 14 $\mu$s [14] 1.5 $\mu$s. The current tail time are also reduced from several tens microsecond [14] to about 10 $\mu$s. On the other hand, the current tail value, which is about 10% of the anode current for the GTO, is now two times as high for the ETO1045S. The overall turn-off loss of the ETO, as shown in Table I, is about the same as that of the GTO under the same snubber condition, while the turn-on loss is significantly reduced. Fig. 7 shows the ETO turn-off energy for ETO1045S at 125C at different anode currents. The turn-off energy increases linearly as the anode current increases. The snubberless turn-off energy is only slightly higher than that with a $dv/dt$ snubber. This is another indication of the high speed capability of the ETO.

The turn-on transient is also accelerated significantly in the ETO and the turn-on switching loss is also reduced as compared to the GTO, as shown in Table I. These are due to the high turn-on current injection [10] from the gate driver with a reduced injection loop stray inductance. In the case without $dv/dt$ snubber, there is no discharge current from the snubber capacitor during turn-on; thus the turn-on energy is further reduced. At 2.5 kV dc link voltage and 0.8 kA current, the turn-on loss is less than 0.15J per pulse.

From Table I, the turn-off time $t_{gq}$, defined as the storage time plus the fall time, for different GTO's varies from 12–14 $\mu$s; while for different ETO's, it varies from 2.3–2.0 $\mu$s. The absolute difference among device's storage time is reduced significantly. The ETO can therefore be considered to have uniform turn-off transient, hence paralleling ETO's becomes relatively easy. Fig. 8 shows the relationship between the storage time, the turn-off time as a function of the turn-off current for the ETO2045S. The storage time does not increase significantly when the anode current increases.

For a traditional GTO, the maximum turn-off current is generally low compared to its maximum RMS current, especially to its surge current capability. This limitation poses a heavy burden on applications to avoid a turn-off operation at higher current. With a better RBSOA, the ETO has a significantly higher turn-off current at the same condition. Fig. 9 shows the

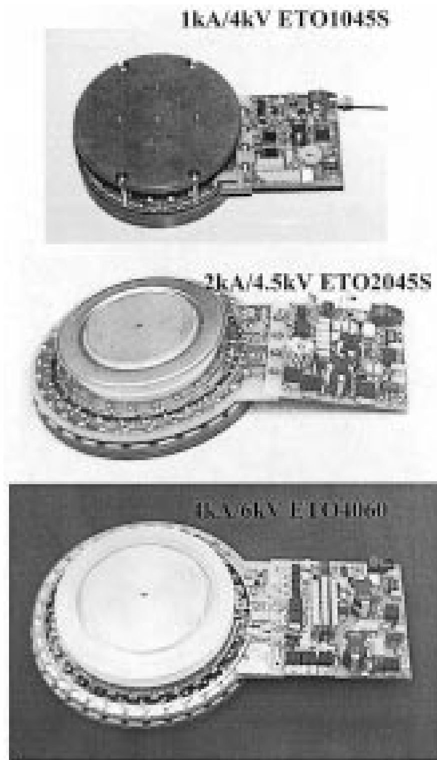


Fig. 5. ETO family and their gate driver.

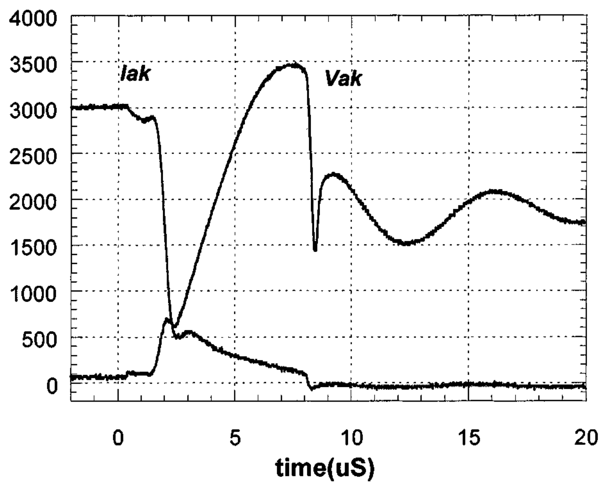


Fig. 6. ETO4060 turn-off characteristic at 25oC.

TABLE I
THE 53 mm GTO AND ETO TEST RESULTS COMPARISON

| | $t_f$ | $t_{gq}$ | $E_{off}$ | $I_{tail}$ | $t_d$ | $t_{gt}$ | $E_{on}$ |
|---|---|---|---|---|---|---|---|
| GTO1 | 1.2 | 14 | 1.93 | 116 | 1.1 | 3.5 | 0.416 |
| ETO1 | 1.0 | 2.3 | 2.1 | 200 | 0.5 | 2.5 | 0.31 |
| GTO2 | 1.3 | 14 | 1.93 | 121 | 1.0 | 3.3 | 0.366 |
| ETO2 | 0.9 | 2.3 | 1.9 | 250 | 0.5 | 1.8 | 0.27 |
| GTO3 | 1.2 | 14 | 1.73 | 111 | 1.0 | 3.2 | 0.349 |
| ETO3 | 0.9 | 2.2 | 2.0 | 250 | 0.5 | 1.6 | 0.26 |
| GTO4 | 1.4 | 13 | 1.69 | 103 | 1.1 | 3.4 | 0.370 |
| ETO4 | 0.7 | 2.1 | 0.95 | 200 | 0.4 | 1.6 | 0.22 |
| GTO5 | 1.1 | 13 | 1.69 | 100 | 1.1 | 3.6 | 0.397 |
| ETO5 | 0.9 | 2.1 | 1.6 | 200 | 0.5 | 1.7 | 0.25 |
| GTO6 | 0.7 | 12 | 1.49 | 147 | 1.1 | 3.6 | 0.425 |
| ETO6 | 0.8 | 2.0 | 1.0 | 200 | 0.4 | 1.7 | 0.32 |

(Anode current 1kA, DC link voltage ~1.8kV, 2μF dv/dt snubber, 120A/μsec di/dt snubber, 125C)

tf: current fall time during turn-off; tgq: turn-off time;
Eoff: turn-off energy; Itail: maximum tail current;
td: turn-on delay time; tgt: turn-on time;
Eon: turn-on energy.

ETO1045S turns off two times as much current as for the GTO at the condition set for the GTO.

The MOSFET has positive temperature coefficiency on its forward voltage drop and normally the GTO has negative temperature coefficiency. By series connecting them together, the ETO shows positive temperature coefficiency in its forward voltage drop like the MOSFET. Fig. 10 shows the measured forward voltage drop versa temperature. For the GTO, the forward voltage temperature coefficiency turns from negative to positive at around 900 A; but for the ETO, this cross over point drops down to below 500 A. This feature again will enable the paralleling of ETO's.

## IV. INVESTIGATION OF THE UNITY TURN-OFF GAIN

The improvement in the ETO's turn-off capability is a direct result of the unity turn-off gain of the ETO. To confirm that the ETO does indeed operate under a unity turn-off gain condition, one has to measure either the emitter or the gate current in addition to the measurement of the anode current. This is almost impossible without introducing a significant amount of inductance in the device, which, by design, is to minimize any inductance within the gate and emitter loops. For this reason, numerical and experimental analyzes were carried out to confirm the unity turn-off gain in the ETO.

TABLE II
SUMMARY OF TYPICALLY ETO TURN-OFF PARAMETERS

| | ETO1045S | ETO2045S | ETO4060 |
|---|---|---|---|
| Voltage rating | 4000V | 4500V | 6000V |
| Current rating | 1000A | 2000A | 4000A |
| Turn-off storage time | 1.5usec | 1.5usec | 1.8usec |
| Turn-off fall time | 0.5usec | 0.5usec | 0.7usec |
| Current tail time | ~10usec | ~10usec | ~10usec |
| Test condition | 1200A turn-off current<br>3500V peak turn-off voltage<br>3u dv/dt snubber | 2500A turn-off current<br>3500V peak turn-off voltage<br>3u dv/dt snubber | 3700A turn-off current<br>3500V peak turn-off voltage<br>3u dv/dt snubber |

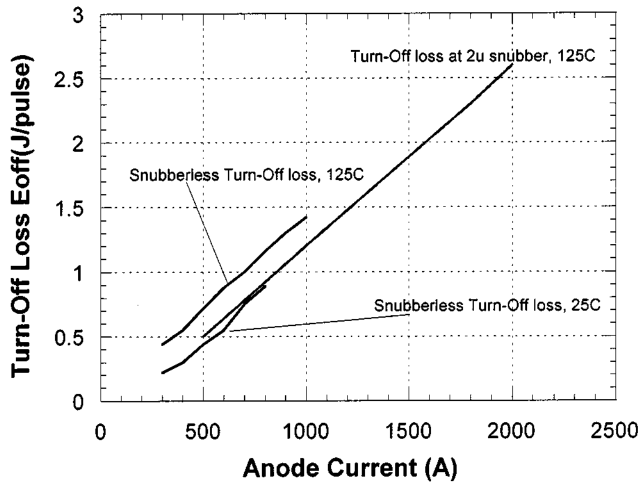


Fig. 7. ETO1045S typical turn-off energy at 1800 V dc link voltage.

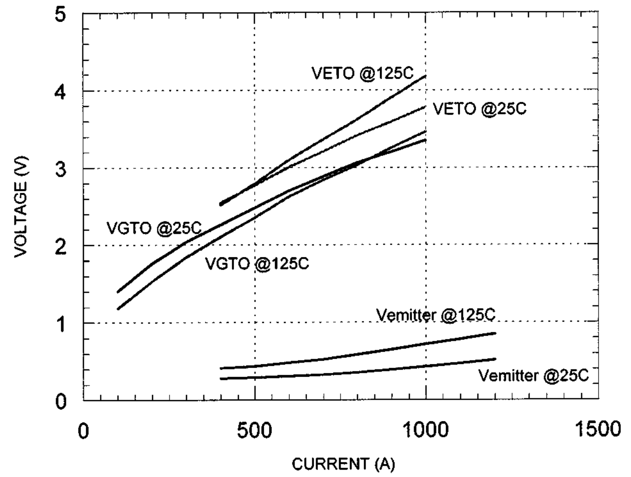


Fig. 10. Relationship of forward voltage drop versa temperature for ETO1045S.

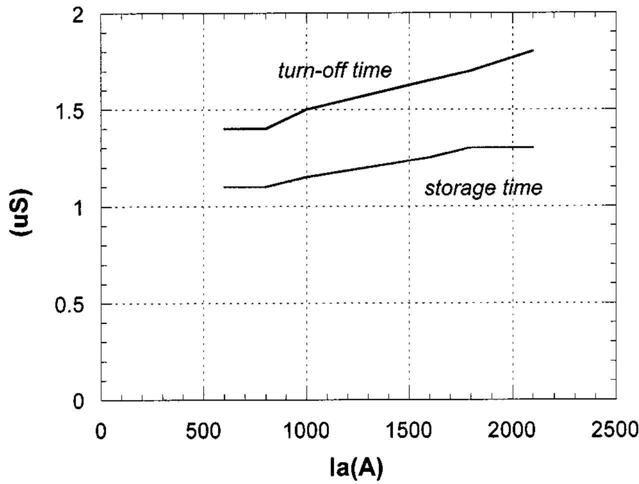


Fig. 8. The turn-off time versus turn-off current for ETO2045S at 3 $\mu$F snubber, 25oC.

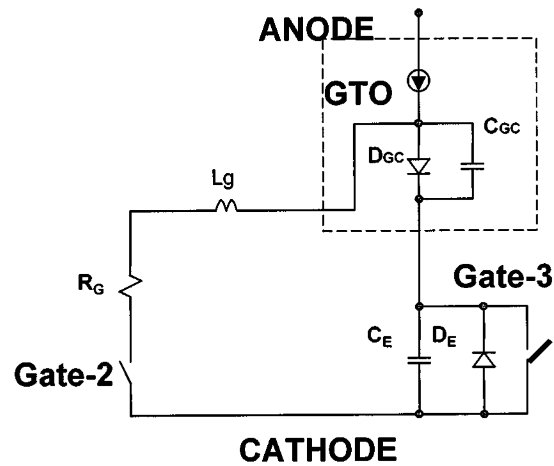


Fig. 11. The equivalent circuit model for the ETO turn-off.

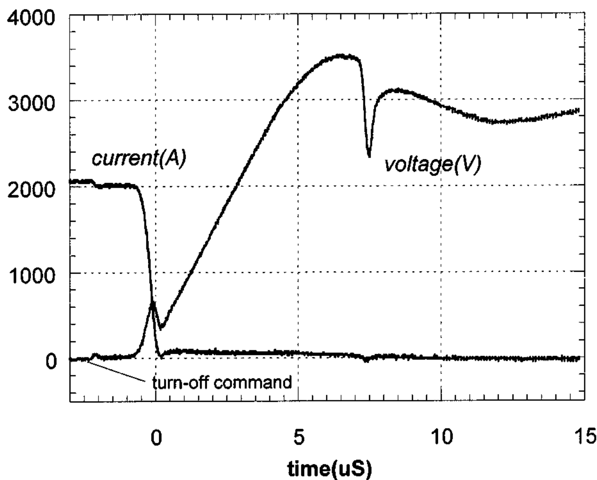


Fig. 9. ETO1045S exhibits two times maximum turn-off current capability.

In actual ETO turn-off, the current commutation from the emitter to the gate is complicated by the high $di/dt$ involved in the process and the unavoidable stray inductance in the package. Therefore, the interaction between the emitter switch $Q_E$, gate switch $Q_G$, and any stray inductance presented in the emitter-gate loop determines the actual performance of the ETO.

Fig. 11 shows the equivalent circuit of the current commutation loop of the ETO during the transient when the GTO's cathode current transfers to its gate loop. The upper PNP transistor in the GTO is modeled as a current source because, during the current commutation stage, the anode current $I_A$ remains almost constant and the PNP transistor operates in a deep saturation region. The emitter junction of the GTO is modeled as a diode $D_e$.

At the beginning of the turn-off process, the emitter MOSFET $Q_E$ is turned off. The emitter switch voltage $V_e$ rises because a constant emitter current, $I_e$, charges the output capacitance of $Q_E$. $V_e$ increases almost linearly until it reaches a preset clamp voltage $V_c$ ($V_c$ is controlled by a clamp circuit in the driver board and is below the breakdown voltage of switch $Q_E$). Because of the relatively small $Q_E$ output capacitance and large charging current $I_e$, this process finishes within 100 ns.

Once the voltage on $Q_E$ increases, the voltage on the emitter diode $D_e$ also increases. Before the charge associated with $D_{GC}$

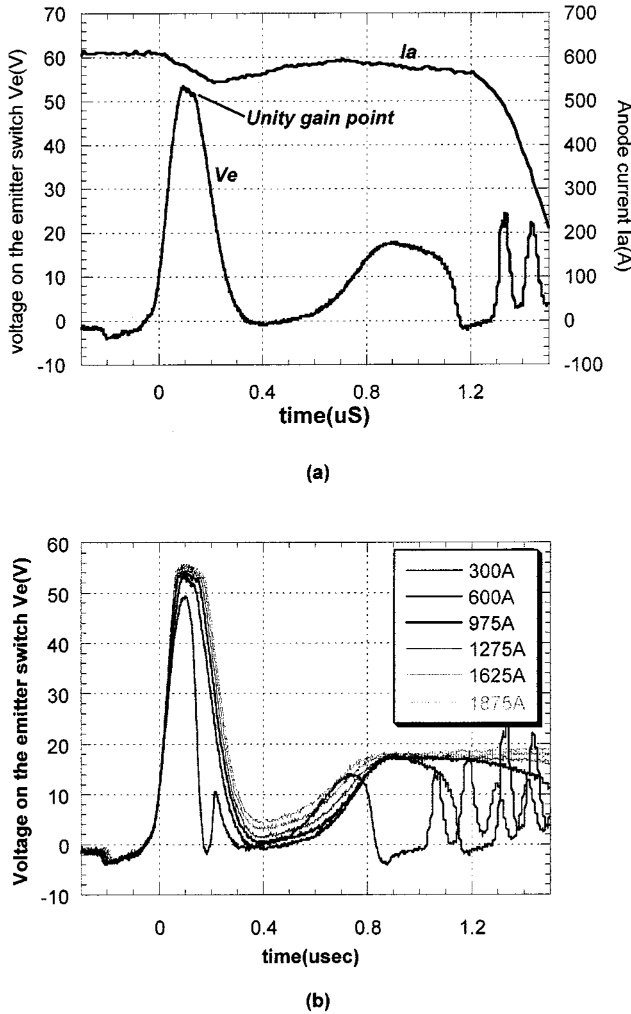


Fig. 12. Dynamic voltage at the emitter MOSFET during ETO turn-off: (a) the emitter MOSFET drain voltage and the ETO anode current and (b) the emitter MOSFET drain voltage at several different turn-off currents.

is removed, $D_{GC}$ can be considered a short circuit. Thus, at the end of this voltage rise phase, a voltage source $V_c$ can be considered to be applied across the gate stray inductor $L_g$ and gate switch $Q_G$, resulting in the charging of the gate current $I_g$. During this phase, the voltage $V_c$ remains constant, and the $dI_g/dt$ in the gate loop is also a constant. The latter can be calculated as

$$dI_g/dt = (V_C - V_{QG})/L_g$$

where the $V_{QG}$ is the forward voltage drop on the gate switch $Q_G$. At the moment the gate loop current $I_g$ reaches the anode current $I_a$, emitter current $I_e$ becomes zero; that is to say, the emitter diode $D_{GC}$ at this moment goes through zero current crossing point and enters a reverse recovery process. Since the emitter junction diode $D_{GC}$ in a high voltage GTO is relatively slow and has a large junction area, it will still act as a short circuit when the current starts to reverse direction. The energy stored in the output capacitor of $Q_E$ is discharged through the reverse recovery current of the $D_{GC}$, resulting in the rapid decrease of the emitter voltage $V_e$. This process also happens very quickly because of the small capacitance value of $Q_E$. The rate of the voltage drop is very much similar to the rate of rise during the charging phase of $L_g$. The voltage will decrease to a value close to $V_{QG}$, and the gate current could become larger than the anode current during this phase because of the discharge current of $Q_E$ output capacitance (or the reverse recovery current of $D_{GC}$).

Based on these analyzes, it is therefore proposed that the instant [as shown in Fig. 12(a)] when the voltage on the emitter switch begins to decrease rapidly from the clamp voltage is the point where the unity turn-off gain is achieved. If this time instant is reached before the ETO anode voltage $V_a$ starts to rise, the device has unity turn-off gain. Another way to say this is that the recovery of the emitter junction ($D_{GC}$) happens earlier than that of the main blocking junction in the GTO.

Fig. 12 shows experimentally observed voltage waveforms on the emitter switch $Q_E$ in ETO1045S during the turn-off at several different anode currents. The anode voltage waveforms (not shown in the figure) show that the anode voltage starts to rise at about 1.2 $\mu$s for the 600 A case. Based on the above analyzes, the gate loop stray inductance $L_g$ in the ETO1045S can be estimated as below. Using the 600 A anode current case as an example, the time it takes for the emitter switch voltage $V_e$ to reach the clamped voltage of 55 V is 0.12 $\mu$s. Assuming the voltage drop across the gate switch $Q_G$ is 10 V, so

$$\begin{aligned} dI_g/dt &= 600/0.12 = 5 \text{ kA}/\mu\text{s} \\ L_g &= (V_c - V_{QG})/dI_g/dt = 9 \text{ nH}. \end{aligned}$$

Since the typical turn-off storage time of the ETO is about 1.52 $\mu$s, it can be concluded, based on the above estimation, that the ETO technology based on traditional GTO parts has a small enough gate stray inductance so that the unity turn-off gain can be fully achieved.

The unity turn-off gain theory described above is also confirmed by an extensive two-dimensional mixed mode device simulation that models the stray inductance as well as the two dimensional carrier distribution in a practical high voltage GTO structure. An inductive switching circuit that resembles the actual test condition of ETO1045S is constructed and simulated using MEDICI [15]. The simulated circuit is shown in Fig. 13. All elements except the GTO are modeled by their lump circuit models. The GTO is modeled by solving basic semiconductor equations. Fig. 14(a) shows the anode voltage and current waveforms obtained from the simulation when the device turns off 1.2 kA at 1 kV. Fig. 14(b) shows the corresponding voltage and current waveforms at the gate and the emitter. Current flowlines that correspond to different time instances during the device turn-off are shown in Fig. 15 around the emitter junction region of the GTO.

Simulation results shown in Figs. 14 and 15 confirm that the unity turn-off gain theory presented herein is correct. The linear increase of the gate current during the first phase of the device turn-off is clearly shown in Fig. 14(b). During the gate current rise phase, the GTO gate voltage is about 0.7 V higher than that of the emitter voltage because $D_{GC}$ is still conducting. Once the gate current reaches that of the anode, both gate and emitter voltage starts to decrease to about 10 V corresponding to the

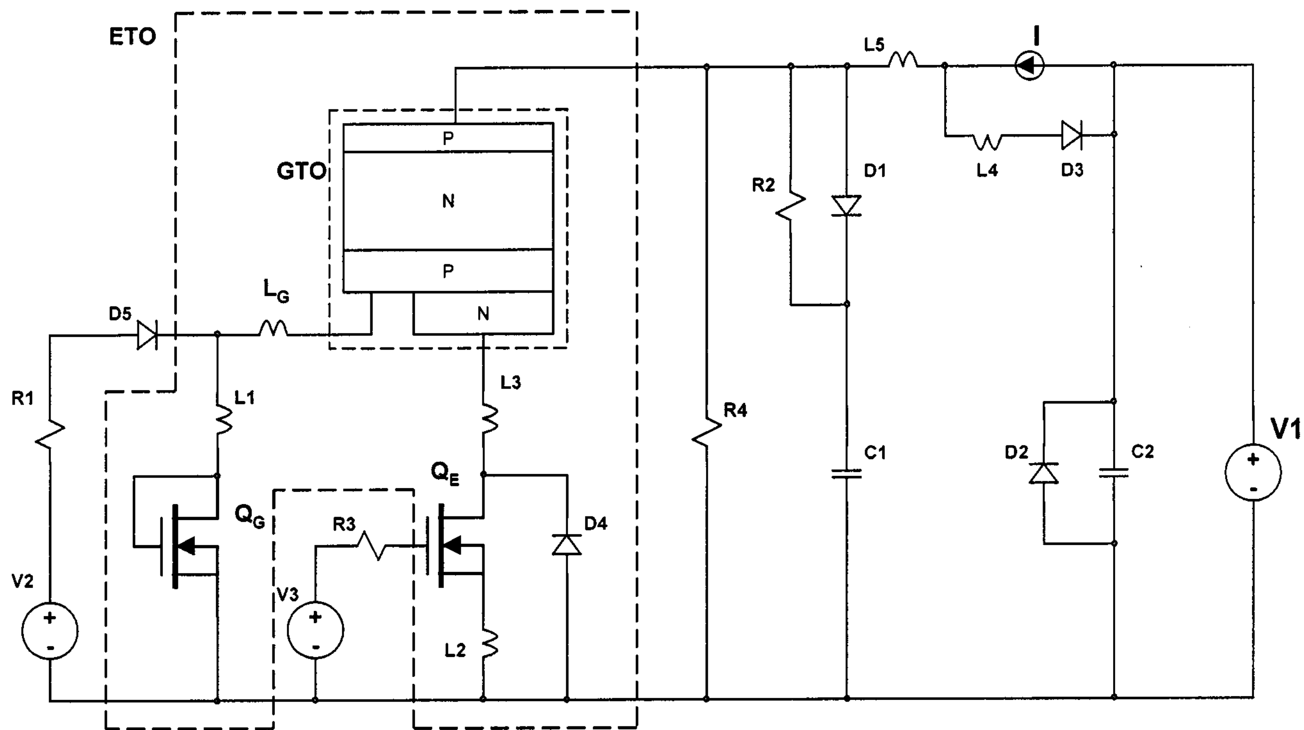


Fig. 13. Circuit used in the mixed mode numerical analysis of the ETO.

voltage required to maintain the high gate current in switch $Q_G$. This simulation shows that the unity turn-off gain is reached within about 600 ns. It takes another 600 ns for the GTO to turn off. A slow increase of the gate current after the first fast rise is caused by the discharge of the snubber capacitor $C_s$ [this also appears as a slow increase in the anode current in Fig. 14(a)].

Inspection of Fig. 15 together with Fig. 14 provides much more needed insights into the ETO operation. During the time when the gate current is increasing, the emitter current is decreasing. This decreasing of emitter current actually happens in a nonuniform manner. Part of the emitter junction close to the gate terminal actually starts reverse recovery much earlier than the part located far away from the gate [Fig. 15(b) and (c)]. The two different current directions in the emitter result in a net decrease of the emitter terminal current. At $t = 0.65$ $\mu$s, the two current components equal each other and the net terminal current is zero. This is the point when unity turn-off gain is reached. At $t = 1$ $\mu$s, the PNP transistor still remains in the saturation mode, but the emitter junction has been fully recovered with no current components through it. However, strong current crowding near the center of the device and near the emitter/gate boundary can still be seen. This is due to the minority carriers still stored in the upper base region of the GTO. Only after all of these charges are removed would the GTO start to turn off. This process takes another 600 ns to complete. At the end of that process, the main anode current decreases rapidly, as does the gate current. The rate of the current decrease depends on, to the first order degree, the gain of the NPN transistor. The current will decrease to a tail current value sustainable by the open base PNP transistor operation, which depends on the charges still remaining in the PNP base and the gain of the PNP transistor. Because ETO's turn off within 1.5 $\mu$s, the charge in the lower PNP transistor is close to its steady state value, resulting in higher tail current value, as shown in Table I. At $t = 5$ $\mu$s, which corresponds to the current tail stage of the device, a very uniform current conduction is seen while the voltage across the main junction reaches the bus voltage.

Another important phenomenon that happens in the ETO is the avalanche breakdown of the emitter gate junction during the rapid fall of the main anode current. As is shown in Fig. 14(b), the rapid falling of the anode and gate current results in a negative voltage at the gate node due to the energy stored in the stray inductance $L_g$. Initially the emitter voltage follows the fall of the gate voltage. However, due to the existence of a body diode in switch $Q_E$, the voltage of the emitter terminal is clamped to about $-0.6$ V, forcing the emitter gate junction of the GTO to be reverse biased. This reverse biased voltage will reach the avalanche breakdown voltage of the emitter/gate junction. The avalanche process lasts until the energy stored in inductance $L_g$ is dissipated in the emitter/gate junction and switch $Q_G$.

As a direct result of the unity turn-off gain, the ETO's RBSOA can be expanded to silicon's $200 \sim 300$ kW/cm$^2$ avalanche breakdown level. For the above mentioned 1 kA/4 kV ETO1045S, the die area is 13 cm$^2$, so it should withstand 1kA snubberless turn-off at its rated voltage. Fig. 16 shows the snubberless turn-off characteristics of ETO1045S. The peak power level is 3.0 MW, or about 230 kW/cm$^2$.

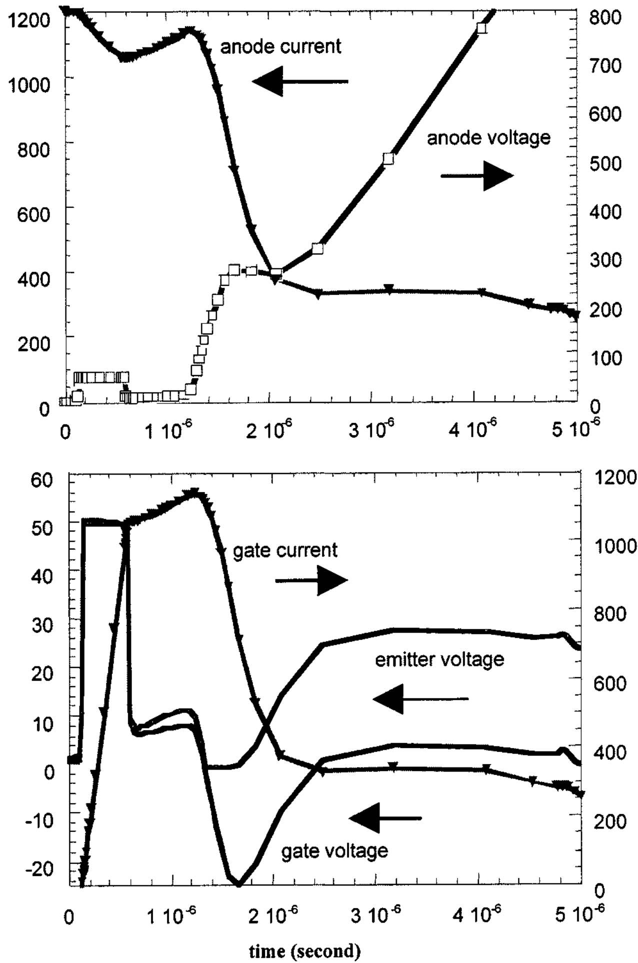


Fig. 14. Results obtained from the mixed mode device simulation: (a) anode voltage and current and (b) gate voltage, gate current, and emitter voltage.

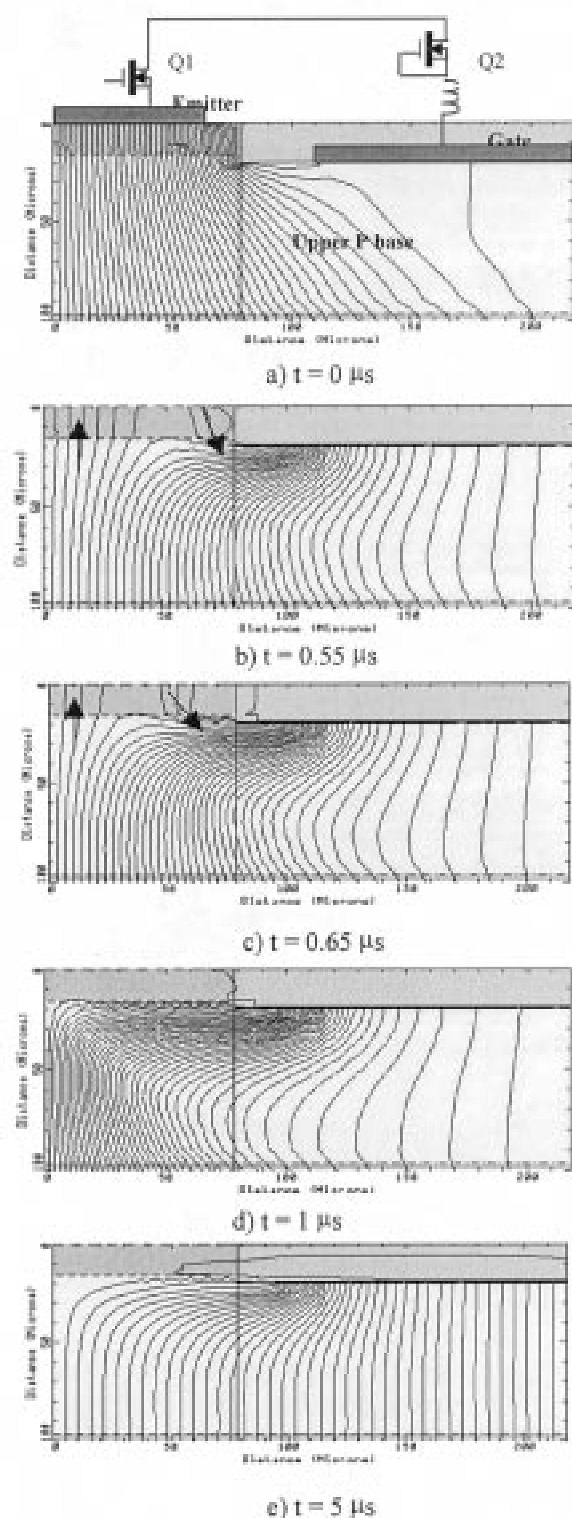


Fig. 15. Current flowlines in the ETO at different time instances during the turn-off.

## V. Comparison of the ETO, IGBT, and IGCT

The IGBT is becoming the most favored power device in industry applications because of its high speed, wide RBSOA, voltage control capability, active $di/dt$ control and over current protection. In the high power area, however, its transient processes become longer, and reliability problems related to its wire-bondpackaging technology become remarkable [16]. The recently introduced IGCT—a specially designed GTO—on the other hand, has improved both switching speed and RBSOA, and thus has the ground to compete with IGBT's in every aspect. Table III summaries important characteristics of these three high power devices at similar power levels.

The comparison is based on the available devices. Right now, 1200 A/3300 V are the highest ratings for the IGBT, while the ETO/IGCT used for the comparison are low rating device in their own categories.

### A. Switching Speed and Forward Voltage Drop

The switching speed is no longer an advantage for the IGBT at high power level. Theoretically, the turn-off process of an IGBT is also an open base PNP transistor turn-off, similar to that of ETO's and IGCT's; all of them should have similar transient behaviors and speeds. On the forward conduction respect, the PNPN latch-up cell in the GTO gives both the ETO and the IGCT lower forward voltage drop than that of the IGBT. The ETO has a higher voltage drop than the IGCT because of the added series switch. It should also be pointed out that the IGCT and IGBT devices compared in Table III have their optimized $N$ base thickness while the ETO does not.

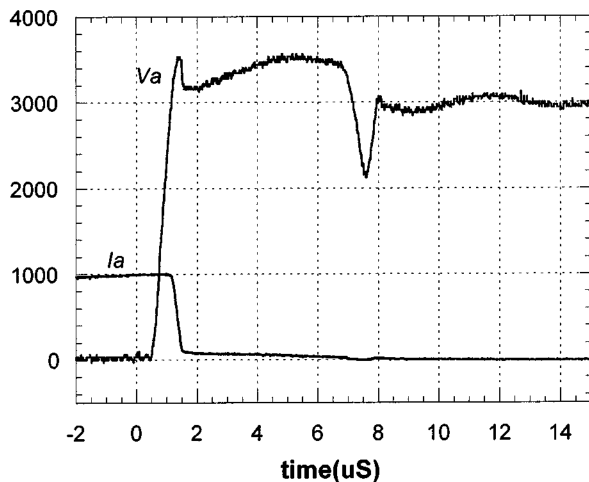


Fig. 16. Snubberless turn-off characteristics of ETO1045S @ 25oC.

### *B. On Device Current Sensing and Over-Current Protection*

The ETO has an important merit that both IGBT and IGCT do not have—the on-device over-current detection capability. The emitter switch of the ETO acts as a small linear resistor in the normal conduction mode, hence the voltage drop across the emitter switch $Q_E$ reflects the current through the device and can therefore be used for feedback and protection purposes. The on-device current sensing through the emitter switch, combined with the fast turn-off speed and high maximum turn-off current, can provide the much needed over-current protection for the ETO. Fig. 17 shows the on-device current sensing configuration. In the ON state, the voltage across the emitter switch reflects the main current through the device and will be less than one volt in the normal conduction mode. Via an R/C low pass filter, any over current can generate an effective voltage output from the comparator and thus generate protection logic through the control logic unit.

Fig. 18 shows the experimental waveforms when an over current detection at almost 800 A was detected. The time required to shut down the ETO when an over current is detected is about 1.5 $\mu$s, which is basically the storage time of the ETO.

The over-current protection for the IGBT is normally realized simply through its current desaturation capability in the active region. This function is also realized on the gate driver board, so that fast response is guaranteed. For the IGCT, over-current protection can only be realized by an outer loop control command initiated by an external over current sensor. Deliberately designed current sensing and feedback circuits are hence required.

### *C. $di/dt$ Control*

One of the most attractive aspects of the IGBT is its active $di/dt$ control. By controlling the rising and/or falling speed of its gate voltage, the IGBT by itself can control the dynamic $di/dt$ in the switching transient. At the expense of higher turn-on loss, the IGBT system can therefore control the reverse recovery of the diodes during turn-on and control the voltage spike during turn-off without passive snubbers. For the IGCT system, external $di/dt$ snubbers is still necessary to accommodate its own $di/dt$ capability and the reverse recovery of the diode. However, in high power systems, the use of $di/dt$ snubber sometimes is dictated by the need to reduce the turn-on loss.

Simulation results predict that the ETO has similar current saturation capability as the IGBT. So the ETO will also have the active $di/dt$ control capability, resulting in the eliminating or saving of the $di/dt$ snubber.

### *D. $dv/dt$ Capability*

A high $dv/dt$ can introduce a voltage on the IGBT's gate through the Miller capacitance and thus turn on (or off) the device by fault. A negative voltage is normally required to drag the gate voltage far below its threshold value, and a low inductance gate control loop is required to absorb the high frequency $dv/dt$ current from the Miller capacitance. Once the gate driver is powered off, the gate driver shows high impedance; the IGBT is thus extremely sensitive to the $dv/dt$. With powered gate driver, the IGCT can stand high $dv/dt$ [17]. However, without power in the gate driver, the gate terminal in the GTO is actually floating, so the IGCT suffers an even worse $dv/dt$ problem, similar to the case of a GTO. The ETO is normally free of the $dv/dt$ problem. No matter the gate driver is powered on or off, the ETO can always bypass its $dv/dt$ current through the gate switch $Q_G$, because the gate switch is turned on automatically.

### *E. Gate Driver*

Due to the voltage control, the gate driver required for the ETO is reduced greatly compared to the GTO. The experimental gate drivers designed for kilohertz applications are shown in Fig. 5. These drivers contain an on-board isolation power supply, an optical-fiber interface, and the required driving capability. The prototype gate driver for the 1 kA/4 kV ETO1045S has a dimension of 2.5 by 2.8 in. Compared to the IGBT's driver, the ETO driver is slightly complex and consumes more power due to the turn-on current injection requirement.

The gate driver is very important to the performance of the IGCT. Its unity turn-off gain is completely determined by the performance of the gate driver and the gate loop stray inductance. The passive components on the driver board are required to conduct very high pulse current. Besides, its gate driver consumes a lot of power, and the power requirement is linearly related to its operation frequency. At 500 Hz, the gate driver for a 4 kA/4.5 kV IGCT requires more than 100 W.

### *F. Serial and Parallel Connection*

The ETO can be used for series and parallel connection. With the unity turn-off gain, the storage time of the ETO is directly determined by the anode current and the gate charges, so it is uniform either among different devices or at different current levels. Fig. 8 shows the relationship between the turn-off time and the anode current. On the contrary, the storage time of the IGCT is theoretically related to its gate driver, the reliability of electrolytic capacitors, gating voltage and the stray inductance

TABLE III
IGBT, IGCT, AND ETO COMPARISON

| | ETO | IGCT | IGBT |
|---|---|---|---|
| **Device** | **ETO1045S** | **5SGX14H4502** | **CM1200HA-66H** |
| **ratings** | **1000A/4500V** | **1560A/4500V** | **1200A/3300V** |
| **Forward voltage drop @1200A, 125C** | **4.2V** | **3.0V** | **4.8V** |
| **Turn-off storage time @1200A, 1650V, 125C** | **1.5u** | **1.0u** | **2.5u** |
| **Turn-off fall time @1200A, 1650V, 125C** | **0.5u** | | **1.0u** |
| **Turn-off loss @ 1200A,1650VDC,125C** | **1.55 J/pulse** | **1.8 J/pulse** | **1.2 J/pulse** |
| **Turn-on loss @ 1200A,1650VDC,125C** | **0.15 J/pulse with di/dt snubber** | **0.18 J/pulse with di/dt snubber** | **2.0 J/pulse without di/dt snubber** |
| **Active control of di/dt & dv/dt** | **possible** | **NO** | **YES** |
| **di/dt snubber requirement** | **YES** | **YES** | **NO** |
| **Active short circuit limitation** | **YES on-device current sensing** | **NO** | **YES desaturation** |
| **Gating power requirement** | **low** | **high** | **Very low** |
| **Gate driver complexity** | **Current turn-on, voltage turn-off on-device current sensing very simple** | **Current turn-on/turn-off complex** | **Simple voltage control** |
| **Transient performance dependency on the gate driver** | **low** | **Unity turn-off gain and storage time are greatly dependent on the gate driver high** | **low** |
| **Parallel operation** | **ETO has positive temp. co-efficiency YES** | **NO** | **YES** |
| **Series connection** | **YES transient behavior is relatively independent of the gate driver, it very good.** | **YES device & gate driver long term transient parameters matching is very important** | **YES** |
| **Snubberless turn-off** | **YES only subject to the avalanche power constant** | **YES only subject to the avalanche power constant** | **YES only subject to the avalanche power constant** |
| **Maximum available device ratings** | **6000A/6000V** | **4000A/4500V** | **1200A/3300V** |

in the commutating loop. Therefore, the ETO has a more uniform transient process than the IGCT, thus is better for serial and parallel operation.

### *G. Operating Frequency*

Medium power IGBT's can work at very high frequency. However, due to the high switching loss, very high power IGBT's are normally used in the system operating around 1–5 kHz.

With a better RBSOA and higher maximum turn-off current, the traditional RCD $dv/dt$ snubber can be scaled down or even removed. This will shorten the turn-off transient. Combined with the reduced turn-on transient process, the maximum operating frequency permitted for the IGCT and the ETO is thus determined mainly by the devices thermal handling capability instead of by the passive components. For the ETO1045S, the maximum operating frequency is around 1 kHz for a three phase 1 MW system.

Soft switching techniques such as the zero voltage transition (ZVT) [18] technology can be used to reduce the switching loss, hence increasing their operating frequency. However, because the gating power requirement is in proportional to the frequency, the IGCT is not as good as the ETO for higher frequency applications.

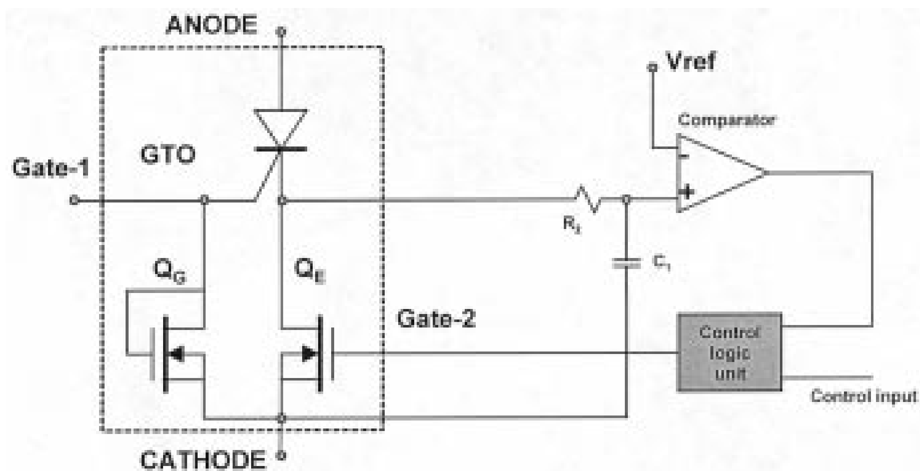


Fig. 17. Over-current protection strategy of the ETO.

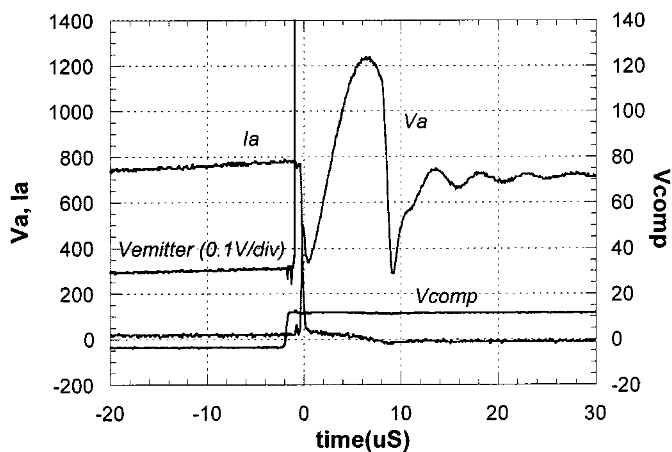


Fig. 18. Over-current protection test waveform. The protection current level is set at 800 A. The time interval between the effective output of the comparator and the main current falling edge is about 1.5 $\mu$s.

## VI. Conclusion

Based on its operation principles, the emitter turn-off (ETO) thyristor has been developed ranging from 1–4 kA, 4–6 kV. The packaging design ensures a very low gate loop stray inductance (about 10 nH for different rating devices), good current sharing, and low thermal resistance. Experimental data proves that the ETO has all of its predicted merits including voltage controlled turn-off capability, high turn-on/off speed, good RBSOA that approaches silicon avalanche limitation. It is a very promising candidate for advanced power conversion in megawatt applications. The root of this new device lies in its hybrid structure, which makes use of both advantages of the GTO and the MOSFET. Further efforts are being made to demonstrate the ETO's capability at system level.

## References

[1] E. R. Motto and M. Yamamoto, "New high power semiconductors: High voltage IGBT's and GCT's," in *Proc. PCIM'98 Power Electron. Conf.*, 1998, pp. 296–302.

[2] D. E. Piccone, R. W. De Doncker, J. A. Barrow, and W. H. Tobin, "The MTO thyristor—A new high power bipolar MOS thyristor," in *Proc. IEEE Ind. Applicat. Soc. 31st Annu. Meeting*, Oct. 6–10, 1996, pp. 1472–1473.

[3] P. K. Steimer, H. E. Gruning, J. Werninger, E. Carrol, S. Klaka, and S. Linder, "IGCT—A new emerging technology for high power, low cost inverters," in *IEEE Ind. Applicat. Soc. Annu. Meeting*, New Orleans, LA, Oct. 5–9, 1997, pp. 1592–1599.

[4] Y. Li, A. Q. Huang, and F. C. Lee, "Introducing the emitter turn-off thyristor," in *Proc. 1998 IEEE Ind. Applicat. Soc. 33rd Annu. Meeting*, 1998, pp. 860–864.

[5] Y. Li and A. Q. Huang, "The emitter turn-off thyristor—A new MOS-bipolar high power device," in *Proc. 1997 VPEC Sem.*, Sept. 28–30, 1997, pp. 179–183.

[6] A. A. Jaecklin, "Performance limitation of a GTO with near-perfect technology," *IEEE Trans. Electron Devices*, vol. 39, pp. 1507–1513, June 1992.

[7] S. Chin and D. Y. Chen, "A GTO circuit using IGT and MOSFET as gate drivers," in *Proc. 1987 IEEE Ind. Applicat. Soc. Annu. Meeting*, 1987.

[8] W. F. Wirth, "High-speed snubberless operation of GTO's using a new gate drive technique," *IEEE Trans. Ind. Applicat.*, vol. 24, pp. 127–131.

[9] J. Oetjen and R. Sittig, "Hybrid 3000A-MOSFET for GTO cascode switches," in *Proc. 1997 IEEE Int. Symp. Power Semiconductor Devices IC's*, 1997.

[10] H. E. Gruening and A. Zuckerberger, "Hard drive of high power GTO's: Better switching capability obtained through improved gate-units," in *Proc. IEEE Ind. Applicat. Soc. 31st Annu. Meeting*, Oct. 6–10, 1996, pp. 1474–1480.

[11] I. Takata, M. Bessho, K. Koyanagi, M. Akamatsu, K. Satoh, K. Kurachi, and T. Nakagawa, "Snubberless turn-off capability of four-inch 4.5 kV GCT thyristor," in *Proc. 1998 IEEE Int. Symp. Power Semiconductor Devices IC's*, 1998, pp. 177–180.

[12] *2-D Device Simulation User's Manual*. Santa Clara, CA: Silvaco International, 1997.

[13] H.-G. Lee, Y.-H. Lee, B.-S. Suh, and D.-S. Hyun, "An improved gate control scheme for snubberless operaton of high power IGBT's," in *Proc. IEEE Ind. Applicat. Soc. Annu. Meeting*, New Orleans, LA, Oct. 5–9, 1997, pp. 975–982.

[14] "GTO data sheet," Westcode Semiconductors Ltd.

[15] *MEDICI User's Manual*. Sunnyvale, CA: Technology Modeling Associates, Inc.

[16] S. Bernet, R. Teichman, A. Zuckerberger, and P. Steimer, "Comparison of high power IGBT's and hard driven GTO's for high power inverters," in *Proc. 1998 IEEE Appl. Power Electron. Conf.*, 1998, pp. 711–718.

[17] "Mitsubishi IGCT data sheet,".

[18] G. Hua, C. Leu, and F. C. Lee, "Novel zero-voltage-transition PWM converters," in *Proc. 1992 IEEE Power Electron. Spec. Conf.*, 1992, pp. 55–61.

**Yuxin Li** (S'98) was born in Hunan, China, in 1964. He received the B.Eng. degree in radio and electronics engineering from Zhejiang University, Hangzhou, China, in 1985 and the M.Eng. degree in semiconductor devices from Nanjing Electronic Devices Research Institute, Nanjing, China and Zhengzhou University, Zhengzhou, China, in 1990.

He has been with the Center for Power Electronics Systems, Virginia Polytechnic Institute and State University, Blacksburg, as a Graduate Research Assistant since 1996. His research interests include switching mode power supplies, high power inverters, and power semiconductor device characterization.

**Alex Q. Huang** (SM'99) received the B.S. degree in electronic engineering from Zhejiang University, Hangzhou, China, in 1983, the M.S. degree in electronic engineering from the Chengdu Institute of Radio Engineering, China in 1986, and the Ph.D. degree from Cambridge University, Cambridge, U.K. in 1992.

He is an Assistant Professor at the Center for Power Electronics Systems, Virginia Polytechnic Institute and State University, Blacksburg. Since 1983, he has been involved in the development of modern power semiconductor devices and power integrated circuits. He fabricated the first IGBT's power devices in China in 1985. While at Cambridge, he developed a high voltage power IC process to integrate power devices and advanced CMOS devices using conventional CMOS technology. His other works include research on monolithic power electronics systems such as the monolithic voltage regulator module (MVRM). He has published more than 70 papers in the international conferences and journals, and has four U.S. patents and more than 10 inventions pending for United States and United Kingdom patents.

Dr. Huang received the NSF Presidential Career Award.

**Kevin Motto** was born in Petersburg, VA, on April 4, 1975. He received the B.S. degree in electrical engineering from the Virginia Polytechnic Institute and State University (Virginia Tech), Blacksburg, in 1997 where he is currently pursuing the M.S. degree in electrical engineering.

Since 1998, he has been with the Center for Power Electronics Systems, Virginia Tech, as a Graduate Research Assistant. He has worked on power electronics for the hybrid electric fuel cell vehicle in addition to researching high power semiconductor devices. His research interests include high voltage thyristor devices as well as inverter drives.